Dynamic behavior of fully solvated β2-adrenergic receptor, embedded in the membrane with bound agonist or antagonist

Peter Spijker*†, Nagarajan Vaidehi*, Peter L. Freddolino*‡, Peter A. J. Hilbers†, and William A. Goddard III*§

*Materials and Process Simulation Center, MC 74-139, California Institute of Technology, Pasadena, CA 91125; and †Department of Biomedical Engineering, Technische Universiteit Eindhoven, 5600 MB Eindhoven, The Netherlands

Contributed by William A. Goddard III, January 5, 2006

Recently we predicted the 3D structure of the human β2-adrenergic receptor (β2AR) and of the binding site of several agonists and antagonists to β2AR. These predictions (MembStruk and HierDock) included no explicit water and only a few lipid molecules. Here we include explicit H_2O and an infinite lipid bilayer membrane in molecular dynamics (MD) simulations of three systems: apo-β2AR, epinephrine-bound β2AR, and butoxamine-bound β2AR (epinephrine is an endogenous agonist, and butoxamine is a β2AR selective antagonist). The predicted structures for apo-β2AR and butoxamine-β2AR are stable in MD, but in epinephrine-β2AR, extracellular water trickles into the binding pocket to mediate hydrogen bonding between the catechol of epinephrine and Ser-204 on helix 5. The epinephrine-β2AR structure shows dynamic flexibility with small, piston-like movements of helices 3 and 6 and transient interhelical hydrogen bonding between Ser-165 on transmembrane 4 and Ser-207 on transmembrane 5. These couplings and motions may play a role in protein activation. The apo-β2AR shows less dynamic flexibility, whereas the antagonist-β2AR structure is quite rigid. This MD validation of the structure predictions for G protein-coupled receptors in explicit lipid and water suggests that these methods can be trusted for studying the mechanism of activation and the design of subtype-specific agonists and antagonists.

The nine human adrenergic receptors all respond to endogenous ligands epinephrine and norepinephrine. These adrenergic receptors are G protein-coupled receptors (GPCRs), in which binding of an agonist in the extracellular region activates a G protein in the cytoplasm. Three of the nine adrenergic receptors belong to the β-subclass of adrenergic receptors, of which β1AR is found mostly in the vessels of cardiac and skeletal muscle and known to cause vasodilation and an increase in cardiac output. The β-blocking drugs were developed to antagonize β1AR for treatment of heart disease. The β2-Adrenergic receptor (β2AR) protein is found predominantly in bronchial smooth muscle, causing bronchodilation when activated. Antiasthma drugs, such as salbutamol, act as agonists to β2AR. Thus, current β-blocking drugs tend to antagonize β2AR, causing a bronchioconstriction risk to asthmatics. Similarly, antiasthma agonists for β2AR may interact with β1AR to cause such side effects as increased heart rate and blood pressure (1). Consequently β2AR has been widely studied resulting in a wide spectrum of pharmacologically well characterized agonists (activators) and antagonists (inhibitors) (2). However, subtype selectivity continues to be a serious issue for these and essentially all other GPCRs.

A major impediment to designing drugs for GPCRs with greater subtype specificity is the lack of a 3D structure for any human GPCR. Consequently, we developed the MembStruk computational method to predict the structure of GPCRs (3, 4), which we validate by predicting the ligand-binding sites on the predicted GPCR using the HierDock ligand-docking method (5). These methods have been applied to several GPCRs (5–9), including the structure and agonist/antagonist binding sites for human β2AR (7). The calculations validating the predicted structure of these ligand–GPCR complexes involve approximations in the treatment of solvent and the lipid membrane that are suitable for a minimized structure but not adequate for describing the dynamics of the receptor/ligand complex so relevant to activation by agonists and efficacy of antagonists (2, 10–14).

In this article we extend the computational model to describe the ligand–β2AR complex by incorporating it into a continuous infinite lipid bilayer membrane (with periodic boundary conditions) while including full solvation with water and salt. Then, starting with the MembStruk–HierDock predicted structures of β2AR with and without bound ligand, we carried out molecular dynamics (MD) simulations on these systems for several nanoseconds. This procedure allows us to validate the stability of the predicted structures and to determine the nature of dynamical effects. We considered three systems:

- apo-β2AR, the MembStruk-predicted structure of β2AR with no ligand bound;
- epinephrine-β2AR, the MembStruk–HierDock-predicted structure of β2AR with the endogenous agonist epinephrine (shown in Fig. 1) bound, and
- butoxamine-β2AR, the MembStruk–HierDock-predicted structure of β2AR with the β2-selective antagonist butoxamine (shown in Fig. 1) bound.

These structures are stable in the MD studies, supporting the accuracy of the MembStruk and HierDock predictions. However, there are some important differences between the various MD simulations. Both apo-β2AR and epinephrine-β2AR exhibit somewhat flexible dynamic structures, whereas the butoxamine-β2AR structure proves to be rigid and stiff. The MD simulation of epinephrine-β2AR shows that water enters the epinephrine-binding cavity to mediate the hydrogen bond between the catechol group of epinephrine and Ser-204 on transmembrane (TM) 5.

We compare these results to experimental results relevant to the process of coupling agonist binding to G protein activation, which is believed to involve motions of several TM helices. Indeed motions of TM3, -5, and -6 have been established to be especially important (12). Experiments show that binding of the ligand to helices 3 and 5 is fast, whereas the motion of helix 6 to bind noncovalently to the ligand takes much longer (12). Helix 6 is believed to undergo either a clockwise rotation to helix 5 or a tilting in the cytoplasmic end toward helix 5. Piston-like movements of helix 6 into the membrane have not (yet) been observed. The time scale of these motions are in the range of nanoseconds (noncovalently binding) to millisec-

Conflict of interest statement: No conflicts declared.

Abbreviations: β2AR, β2-adrenergic receptor; $CRMS_\alpha$, RMS deviation in α carbon coordinates; GPCR, G protein-coupled receptor; MD, molecular dynamics; TM, transmembrane.

‡Present address: Beckman Institute for Advanced Science and Technology, University of Illinois at Urbana–Champaign, Urbana, IL 61801.

§To whom correspondence should be addressed. E-mail: wag@wag.caltech.edu.

www.pnas.org/cgi/doi/10.1073/pnas.0511329103

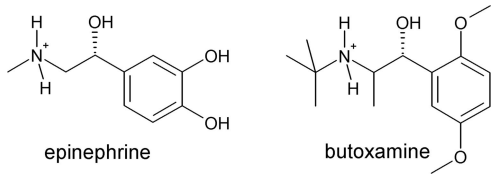

Fig. 1. Ligands used to study binding to the β2-adrenergic receptor. Epinephrine is an endogenous ligand (agonist), whereas butoxamine is an antagonist specific for β2AR.

onds (rigid motions) (10). We find results that are consistent with most of these observations.

Results and Discussion: Changes in the Receptor Conformation During Dynamics

Apo-β2AR Simulations. Comparing the initial structure from the MembStruk–HierDock predictions of apo-β2AR (similar to Fig. 2 *Left*) to the structure after 4 ns of MD simulation in the presence of a full membrane and water, we see some changes in the conformation of the protein, some helices tilting closer to each other, as discussed below, while the loops move substantially. Thus, matching the C_α atoms of the TM helices of the apo-β2AR structure after 4 ns to the original structure for the two sets of MD simulations, gives coordinate root mean square [RMS deviation in α carbon coordinates ($CRMS_\alpha$)] differences of 2.4 Å. In comparison, the $CRMS_\alpha$ for the loops is 6.0 Å and 5.4 Å as expected because these loops are fluxional.

Examining the two apo-β2AR structures over the period of 6 ns, we notice some conformations more suitable for binding agonist [orientation of the OH group of Ser-207 (TM5) toward where the catechol OH of the ligand would be], whereas others are not [orientation of the OH group of Ser-207 (TM5) pointing toward the OH group of Ser-165 (TM4)]. Comparing the two structures with each other after 4 ns with each other, we find a $CRMS_\alpha$ difference of 3.3 Å for the helical regions and 5.0 Å for the loops (due only to their different initial velocities, before the MD), indicating the flexibility of the system.

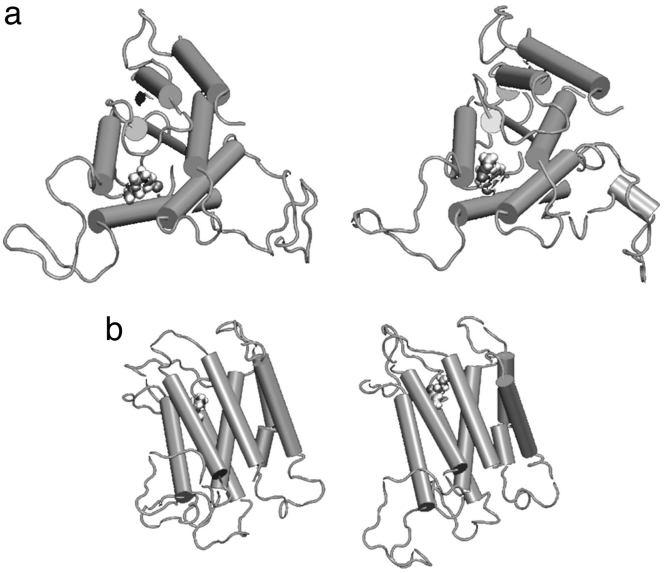

Fig. 2. The structure of epinephrine-β2AR at the start (*Left*) and after 4 ns of MD simulations (*Right*). (*a*) Orthogonal top view. (*b*) Side view. The figure shows that the tilts in helices 3 and 4 increase by an additional 6° and 7° with respect to the surface normal of the lipid bilayer. The protein is shown in a cartoon, and the epinephrine is shown as Van der Waals spheres. The program VMD was used for visualization (15).

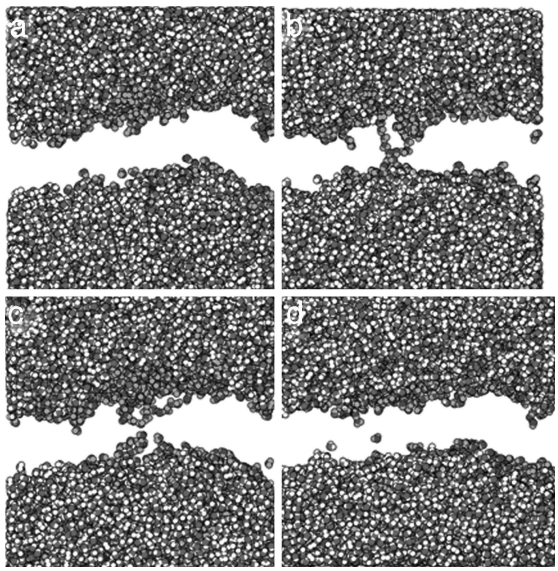

Fig. 3. The structure of the water for the initial structure (*a*) and after 3 ns of MD simulations for apo-β2AR (*b*), epinephrine-β2AR (*c*), and butoxamine-β2AR (*d*). The protein and bilayer are omitted for clarity. The protein is located in the center of each figure.

Butoxamine-β2AR Simulations. With butoxamine-β2AR we observe less motion in the ligand and the helices compared with apo-β2AR (or epi-β2AR), indicating a more rigid structure. Matching the protein structure after 4 ns to the original butoxamine-β2AR structure gives a $CRMS_\alpha$ change of 2.1 Å for the helices and 5.9 Å for the loops. Comparing the butoxamine molecules after 4 ns, we find a RMS difference of 0.3 Å.

Epinephrine-β2AR Simulations. Comparing the initial structure from the MembStruk-HierDock predictions of epinephrine-β2AR (the left half of Fig. 2) to the structure after 4 ns of MD simulation in the presence of a full membrane and water, we see some significant changes in the conformation of the protein with an upward movement of the epinephrine by ≈1.2 Å but not out of the docking cavity. Some helices tilt to become closer to each other, as discussed below. Matching the protein structure after 4 ns to the original structure, the $CRMS_\alpha$ difference is 2.3 Å. This finding shows that the important structural elements of the predicted structure are maintained in the simulation.

However, more significant changes occur in the intracellular (IC) and extracellular (EC) loops. These undergo large deformations, as can be seen in Fig. 2. The $CRMS_\alpha$ differences in these loops range from 3 Å to 5 Å.

Thus comparing the ligand–protein structures for agonist and antagonist, we see that binding of the antagonist leads to a more rigid structure. This increased rigidity may play a role in the mechanism by which an antagonist prevents activation.

Dynamics of Water Through the 7TM Barrel. Fig. 3*a* shows the packing of water in the apo-β2AR-membrane complex at the start of the MD, whereas Fig. 3*b* shows the structure for the apo-β2AR after 3 ns of MD. This shows the formation of a water channel through the central axis of the protein (the TM3, -4, -5, -6 barrel). However, only 1 or 2 water molecules are observed to move through the channel.

Some water channeling, but much less, is observed for epinephrine-β2AR (Fig. 3*c*), whereas no water channel was found for butoxamine-β2AR (Fig. 3*d*). This procedure indicates a more rigid structure for the antagonist than for the agonist and an even less rigid structure for apo-β2AR.

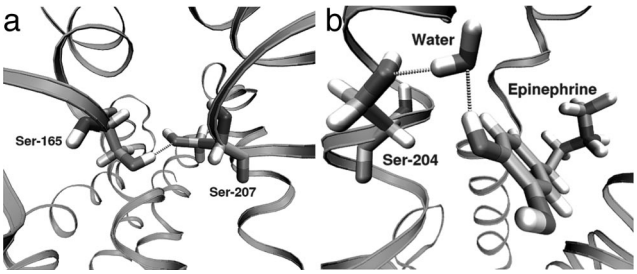

Fig. 4. Structural elements in epinephrine-β2AR. (*a*) The hydrogen bond between Ser-165 (helix 4) and Ser-207 (helix 5), with a length of 2.81 Å. (*b*) The water-mediated hydrogen bond between the *para*-catechol OH of epinephrine and Ser-204 (helix 5). This mediated hydrogen bond has lengths of 2.99 Å (from epinephrine to water) and 2.75 Å (from water to Ser-204). In both figures the hydrogen bonds are depicted by a dotted yellow line, the protein is shown as a ribbon, and the serine residues of interest, the water, and epinephrine are shown as a stick model. Water and the bilayer have been omitted for clarity. The program VMD was used for visualization (15).

We also observed water entering the conserved Asn-51 (TM1)–Asp-79 (TM2)–Asn-322 (TM7) hydrogen bond network in the MD run for apo-β2AR and for epinephrine-β2AR, but not for butoxamine-β2AR.

Role of Water in Mediating the Dynamics of the Interhelical Hydrogen Bonds and Ligand–Protein Hydrogen Bonds. The MembStruk–HierDock predictions contained no explicit solvent. Thus, the explicit water simulations allow us to determine whether explicit water plays an important role. Fig. 4*b* shows that indeed explicit water mediates the hydrogen bond between Ser-204 (TM5) and the catechol OH-group of epinephrine at some time steps during the MD simulations. The first part of the hydrogen bond has a length of 2.99 Å [from epinephrine to the water molecule, measured with VMD (15)], and the second part has a length of 2.75 Å [from the water molecule to Ser-204 (TM5)].

At other times TM5 is oriented to form hydrogen bonds to TM4; for example, Fig. 4*a* shows that at 172 ps a hydrogen bond is formed between Ser-165 on helix 4 and Ser-207 on helix 5, which has a length of 2.81 Å. We consider that the interhelical hydrogen bonds between serines of helices 4 and 5 represent the inactive state before binding of agonist. Binding of the epinephrine competes for some of these same serines of helix 5. Hence, as the agonist enters the binding pocket, helix 5 must rotate counterclockwise to make the hydrogen bond with the catechol groups. Indeed, during the MD we see just some changes with the TM5 orienting more toward TM4 when the ligand moves away (to allow the explicit water to enter), and then the TM5 orients toward the ligand as it moves back (with extra water).

We believe that this and other associated motions might play a role in activation. Indeed, a two-state binding model leading to activation has been proposed by several authors (7, 13). In contrast, we saw little rotation in helix 5 for the antagonist complex and only small fluctuations for the apoprotein.

Thus, the observation of water-mediated hydrogen bonds between helices or between the helix and epinephrine can play an important role in activation, making explicit water calculations an important final step in optimizing the predicted structure. Similarly, such explicit water is likely quite important in determining absolute bonding energies.

Quantitative Analysis of Helical Motion in MD Simulations. In this section we examine the dynamic nature of the nonbond distances to epinephrine from those residues known from experiment to be involved in activation (13). This analysis may allow us to understand the initial events leading to activation of β2AR. The residues for which the distances have been measured experimentally are listed in Table 1. The residues in this table are labeled according to National Center for Biotechnology Information numbering. The residues of interest are Asp-113, Ser-165, Ser-203, Ser-207, and Asn-293 for epinephrine-β2AR, and Asp-113, Hsd-172, Trp-286, and Ile-294 for butoxamine-β2AR. Of course, other residues not listed here also interact with the ligand.

Table 1. The residues of the β2AR that play a role in binding the ligands epinephrine and butoxamine (listed by helix)

Ligand	Helix 3	Helix 4	Helix 5	Helix 6
Epinephrine	Asp-113 Val-117	Ser-165 Ile-169	Ile-201 Ser-203 Ser-204 Ser-207	Phe-290 Asn-293
Butoxamine	Asp-113 Cys-116	Ile-169 Hsd-172	Ser-203	Trp-286 Asn-293 Ile-294 Val-297

The residues in this table are labeled according to National Center for Biotechnology Information numbering.

For hydrogen bonds we report the distance between the hydrogen bond acceptor and the hydrogen atom of the donor. For salt bridges we report the closer distance between an oxygen of the carboxylate group and the nitrogen of the protonated amine. For hydrophobic interactions we report the distance between a carbon atom to the closest hydrogen of the hydrophobic part of the other molecule.

The butoxamine–helix interactions are somewhat similar with those for epinephrine–helix, but butoxamine has fewer hydroxyl groups (see Fig. 1) and fewer hydrogen bonds, and is likely to have more hydrophobic interactions than for epinephrine. Fig. 5 shows the variation with time of nonbond distances between the ligands epinephrine (*Upper*) and butoxamine (*Lower*) and the residues of interest. These figures show that the salt bridge between the Asp-113 (TM3) and the protonated amine is preserved throughout the dynamics for both ligands (arrows 1 and 2 in Fig. 5), leading to an average length of 2.8 Å for epinephrine-β2AR and 3.0 Å for butoxamine-β2AR. On the other hand, the ligand–protein hydrogen bonds fluctuate during the MD. The hydrogen bond between the metacatechol hydroxyl group of epinephrine with Ser-203

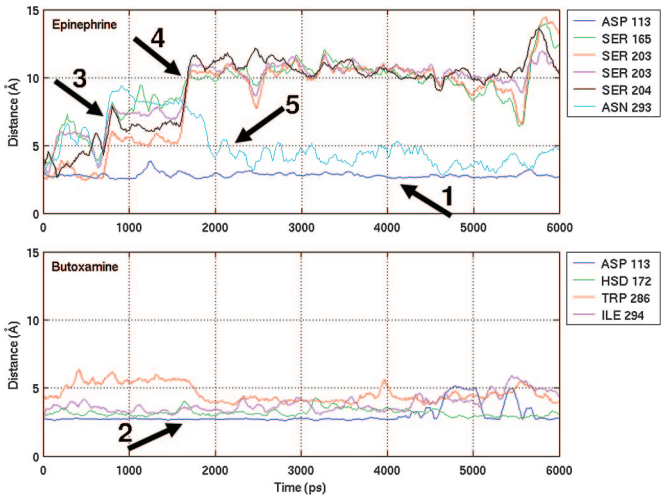

Fig. 5. Variation of nonbond distances with time for several residues in the β2AR. (*Upper*) Epinephrine-β2AR. (*Lower*) Butoxamine-β2AR. The different residues are listed in the legends to the right. For Ser-203, we report the distances to both two OH groups of the catechol moiety of epinephrine. The arrows indicate specific events, which are discussed in the text.

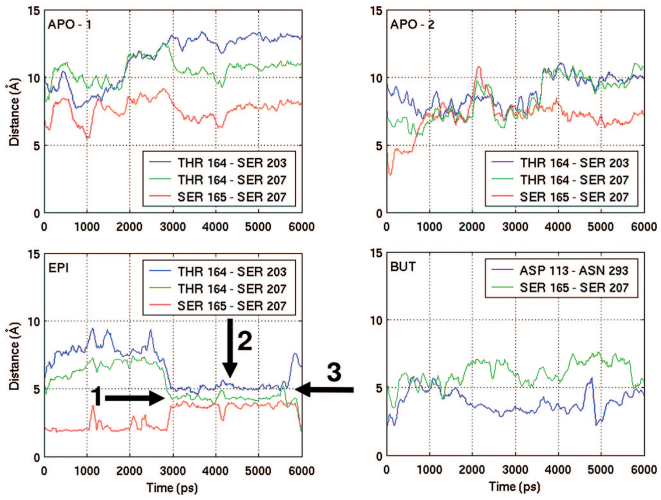

Fig. 6. Interactions between residues residing on different helices for all four simulations. (*Upper*) Lengths of these noncovalent bonds for the apoprotein simulations. (*Lower Left*) Epinephrine simulation. The Thr-164 to Ser-203 interaction is shown in blue, the Thr-164 to Ser-207 interaction is in green, and the Ser-165 to Ser-207 interaction is in red. Residues Thr-164 and Ser-165 are on helix 4, and residues Ser-203 and Ser-207 are on helix 5. (*Lower Right*) Interactions for the butoxamine simulation between Asp-113 on helix 3 and Asn-293 on helix 6 (in blue) and Ser-165 on helix 4 and Ser-207 on helix 5 (in green). The arrows indicate specific events, which are discussed in the text.

(TM5) is maintained as a direct hydrogen bond for ≈0.8 ns (the breakage is indicated by arrow 3 in Fig. 5) and as a water-mediated hydrogen bond for another 0.8 ns (the breakage is indicated by arrow 4 in Fig. 5). The hydrogen bond between Asn-293 and the β-hydroxyl group on the alkyl chain of epinephrine is lost near the beginning of the simulation (arrow 3 in Fig. 5) but forms again after 2 ns (arrow 5 in Fig. 5). Most other hydrogen bonds between TM4 (Ser-165) and TM5 (Ser-204) are lost almost immediately (arrow 3 in Fig. 5).

During the MD simulations, butoxamine continues to exhibit hydrophobic interactions with His-172 (TM4) and Trp-286 (TM5) and Ile-294 (TM6). Fig. 5 shows that these interactions remain tight through the entire MD run. It is found that the hydrophobic interactions with Val-119, Ile-169, and Phe-290 remain rather constant (≈4.5 Å) throughout the MD run.

The nonbond distances between residues on different helices were also analyzed to understand how the dynamics in lipid and water affect the interhelical distances. We find that during the dynamics the Ser-207 (TM5) breaks its hydrogen bond with epinephrine forming instead a hydrogen bond with Ser-165 (TM4) as seen in Fig. 4. This is associated with the rotation of TM5 mentioned above.

Based on visual inspection of the simulation trajectories, we chose to follow the dynamics of certain residues explicitly. The distances between the residues are calculated in the same way as with the lengths of the nonbond interactions between ligand and residue. For the apoprotein and epinephrine–protein simulations, we examined the distances of three pairs Thr-164 to Ser-203, Thr-164 to Ser-207, and Ser-165 to Ser-207 (all between TM4 and -5). Except for the pair Ser-165 to Ser-207, these interactions are not found in the butoxamine simulation. On the other hand, in the butoxamine simulation the pair Asp-113 to Asn-293 (from helix 3 to 6) seems interesting and was investigated. These distances are shown in Fig. 6.

In both the apoprotein and butoxamine–protein simulation, these hydrogen bonds loosen during the MD. However, for epinephrine-β2AR the hydrogen bond between Ser-165 and Ser-207 is conserved for almost 3 ns. It then loosens, but at the same time

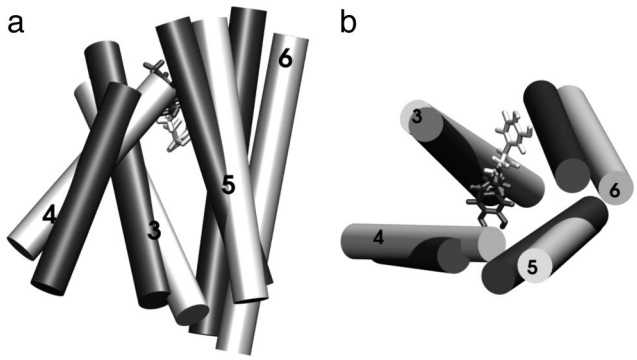

Fig. 7. Schematic representation of the change in helical configuration for the helices surrounding the docking cavity (helices 3–6). (*a*) Side view. (*b*) Top view. The initial configurations are shown in black (also the ligand epinephrine), and the final configurations are shown in white. The remainder of the protein, as well as the bilayer and the water, is omitted for clarity. The program VMD was used for visualization (15).

the distance from Thr-164 (TM4) to both Ser-203 (TM5) and Ser-207 (TM5) tightens considerably (arrow 1 in Fig. 6). For the next 3 ns the distances remain constant, indicating strong interhelical interaction (arrow 2 in Fig. 6). At the end of the simulation the hydrogen bond between Thr-164 and Ser-203 loosens, but the hydrogen bond between Thr-164 and Ser-207 and Ser-165 and Ser-207 tightens, indicating an increase in strength (arrow 3 in Fig. 6). The presence of these interhelical hydrogen bonds in the agonist complex and their absence in the apoprotein and antagonist complex suggest that these interactions induced by the agonist might be important for receptor activation. Recent experiments on rhodopsin (the only GPCR for which a crystal structure is available) also showed the importance of interhelical hydrogen bonding as a step in the protein activation (16).

Fig. 7 shows the helical conformation of the protein for helices 3–6 for the initial (black) and final (t = 6 ns; white) conformations. The side view (Fig. 7*a*) shows that helices 3 and 6 have moved downwards (≈5 Å), and that the intracellular ends of helices 4 and 5 have moved in different directions. The top view (Fig. 7*b*) illustrates the observation made above that the extracellular ends of helices 3 and 6 move apart. This is an important observation, because it is known that the G protein is coupled to the highly conserved DRY-motif (an ASP-ARG-TYR sequence) located at the end of helix 3. The DRY-motif is believed to play an important role in protein activation (17). Thus, the motions observed with respect to helix 3 provide a strong indication that such motions are involved upon in protein activation.

In comparing structures, we have calculated the RMS distance of the helical backbone ($CRMS_\alpha$) in two ways. The absolute $CRMS_\alpha$ gives information on the correlation of a protein structure throughout time with respect to the initial structure to provide some idea about the accuracy of the original structure. The relative $CRMS_\alpha$ gives insight in the dynamical correlation of two in time subsequent structures equilibrated in membrane and water. Both types of $CRMS_\alpha$ are shown in Fig. 8. The $CRMS_\alpha$ values of 1–2 Å for the β2AR structure show that the predicted structure is stable in lipid bilayer. The relative $CRMS_\alpha$ slowly converges to a value of 0.6 Å, indicating the range of dynamical fluctuation in the structure.

Conclusions

These analyses of the fully solvated structures with a complete description of the membrane make it clear that the overall predicted β2AR structures are stable. The helices move somewhat with respect to each other, but there are no large instabilities, and the helical conformations are preserved. Although the structure predictions used only a small lipid barrel, we see only modest changes

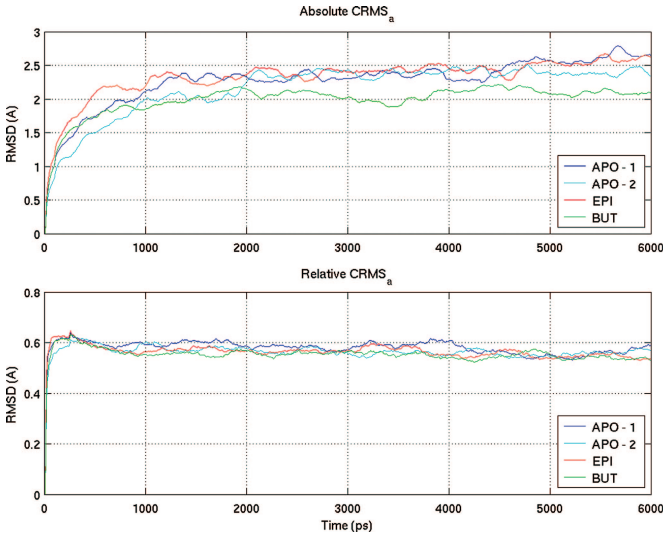

Fig. 8. Backbone root mean square distances (CRMS$_\alpha$) for several sets of simulations. (*Upper*) The absolute CRMS$_\alpha$ (with respect to the first frame). (*Lower*) The relative CRMS$_\alpha$ (with respect to the previous frame).

from including the full membrane in the model. Thus, the CRMS$_\alpha$ comparisons show that the conformations of the β2AR are stable in the native bilayer-water environment. This finding validates the MembStruk procedure, indicating that the MembStruk predicted structures are reasonably accurate. The minor changes in the ligand–protein interaction caused by the presence of water and lipid indicate that including explicit water would have been useful in docking the agonist to the receptor. The behavior of the interhelical loops shows that these loops are very dynamic, as expected, indicating that an ensemble of favorable loop structures should be considered in the docking calculations.

Examination of the MD trajectory indicates that explicit inclusion of water has some significant effects on ligand–residue interactions and that these interactions change dynamically. The strong salt bridge interactions between Asp-113 (TM3) and the protonated amine of both epinephrine and butoxamine are preserved in the dynamics, confirming the importance of this interaction for the fast binding step (12) of the ligand, be it an agonist or an antagonist. The hydrogen bonds between serines on TM5 and epinephrine are slower to form, being water-mediated and dynamic in nature. We observe here an interhelical hydrogen bond between helices 4 and 5 that must break to form the hydrogen bonds with the catechol group of epinephrine. This finding shows that the step of forming hydrogen bonds with the catechol group is slow, involving a competition between forming interhelical hydrogen bonds (the inactive state of the receptor) and forming the hydrogen bonds with the agonist epinephrine (the active state). Thus, the agonist binding and activation involves at least two steps, as observed in the MD: the protonated amine contact with Asp-113 (TM3) is made first followed by rotation of helix 5 to make hydrogen bonds with the catechol of epinephrine. These conclusions drawn from the MD simulations are consistent with similar conclusions by other researchers based on experiments (13, 16).

The motion of helices 3 and 6 downward (see Fig. 7) occurred only with the agonist epinephrine bound and not with either the antagonist bound protein or the apoprotein. The piston-like movements of these helices could be involved in the activation of the protein (10), and the motions we observe probably show the beginning of these piston-like movements.

The changes in the interhelical hydrogen bonding between helix 4 and 5 as the agonist is bound are most interesting. It remains fairly stable throughout the simulation. In addition, the occurrence of water-mediated hydrogen bonds shows that water can play a critical role in ligand binding. The differences in the simulations between the antagonist-protein, the agonist-protein, and the apoprotein structure make it clear that just 6 ns of simulations already show differences between agonist and antagonist that can be compared with experiment. However, longer simulations would certainly contribute to confirm the observed behavior. Thus, we find that antagonist-protein simulations differ substantially from the dynamics of the apoprotein and of the agonist-β2AR systems.

Computational Methods

The Structural Model. The initial 3D structure of the human β2AR was obtained from MembStruk predictions (3, 4, 7), whereas the 3D structures with the ligands epinephrine or butoxamine bound to β2AR were obtained from HierDock predictions (5, 7). The protonated amine of epinephrine forms a salt bridge with the Asp-113 on TM3. The catechol hydroxyl groups form a hydrogen bond network with Ser-203, Ser-204, and Ser-207 on TM5. The β-hydroxyl group in the alkyl chain of epinephrine hydrogen bonds to Asn-293 on TM6. Epinephrine also has hydrophobic interactions with Val-119 on TM3, Ile-169 on TM4, and Phe-290 on TM6.

The butoxamine antagonist, which is larger and more hydrophobic than epinephrine, interacts with such additional hydrophobic residues as Trp-109 on TM3 and Phe-289, Phe-290, and Ile-294 on TM6. The oxygens on butoxamine were involved in hydrogen-bonding interactions with Ser-203 and Ser-204, but there was no interaction with Ser-207 on TM5. There was no direct experimental validation for this binding site. However, the HierDock predictions for several agonists and antagonists gave reasonable relative binding energies (7), and these dynamics studies show very little change in the ligand–protein complex from the predicted binding site. Thus, we believe that the predicted binding site for butoxamine is correct. We consider both epinephrine and butoxamine to be protonated, at physiological conditions.

The butoxamine antagonist, which is larger and more hydrophobic than epinephrine, interacts with such additional hydrophobic residues as Trp-109 on TM3 and Phe-289, Phe-290, and Ile-294 on TM6. The oxygens on butoxamine were involved in hydrogen-bonding interactions with Ser-203 and Ser-204, but there was no interaction with Ser-207 on TM5. We consider both epinephrine and butoxamine to be protonated, at the physiological conditions.

To construct the periodic cell for the MD simulations, the predicted structures of apo-β2AR, epinephrine-β2AR, and butoxamine-β2AR from ref. 7 were each independently embedded in the center of a square periodic lipid bilayer consisting of 200 dipalmitoyl phosphatidyl choline molecules and solvated with ≈15,000 water molecules. The dimensions parallel to the membrane were 92 Å and 80 Å, and the diameter of the protein barrel was 27 Å. The periodic cell measures 100 Å perpendicular to the membrane, and the thickness of the membrane was 38 Å and the total thickness of the protein was 55 Å. To compensate for the net charge of the protein and ligand, eight waters for the apoprotein or nine waters for the ligand-bound protein were replaced by chloride ions to attain a zero net charge for the entire system. The initial structure for epinephrine-β2AR is shown in Fig. 9. These systems contains 76,253 atoms (apoprotein-β2AR), 76,278 atoms (epinephrine-β2AR), and 76,296 atoms (butoxamine-β2AR).

We used the CHARMM22 force field parameters for the protein, the TIP3 model for water (18, 19), and the CHARMM27 force field parameters for the lipids (20). Because not all force field parameters were available for epinephrine and butoxamine in CHARMM, we derived these parameters from parameters already

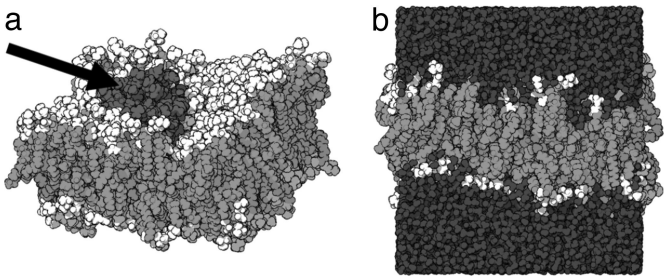

Fig. 9. A schematic view of the epinephrine-β2AR–lipid bilayer water complex. (*a*) A bird's-eye perspective of the complex with all waters omitted. Visible are the protein (red, indicated by the arrow) and the lipid bilayer (green for carbons, and white for head groups). The epinephrine is not visible, because it is in the pocket inside the protein. (*b*) An orthogonal side view of the complex with water in blue. The protein is not visible, because it is inside the membrane and the water. The width of the periodic cell is 92 Å, and the height is 100 Å.

present in the CHARMM force field for similar chemical groups. These new parameters are reported in the supporting information, which is published on the PNAS web site. Minimization of both ligands in vacuum for these ligands led to bond lengths, angles, and dihedrals similar to the quantum mechanical results and the previous structures determined with DREIDING (21). Gasteiger charges were used for these ligands (22).

Simulations Details. Four independent MD simulations, each 6 ns long, were carried out by using the program NAMD 2.5 for all minimization and MD runs (23, 24). Two of these simulations considered only apo-β2AR embedded in the bilayer and solvated in the water (including the chloride ions to account for the net charge). These two apoprotein simulations differ only by having their initial velocities redefined (independent assignment of the Gaussian distributions). The other two simulations were epinephrine-β2AR and butoxamine-β2AR.

The process was first to minimize the water and lipid bilayer while keeping the protein and ligand fixed. This was followed by an all-atom conjugate gradient minimization of the entire system for 20,000 steps. After this minimization, we carried out 5 ps of MD simulations for equilibration (not used for analysis) using 1-fs time steps, followed by 6 ns of MD simulations with the same time step size. Langevin dynamics was used for temperature control with the thermostat set at 310 K. The Nosé–Hoover Langevin piston pressure control was used to control fluctuations in the barostat, which was set at a pressure of 1 bar (1 bar = 100 kPa). Here the periodic cell was constrained to remain orthorhombic, but the cell parameters were allowed to vary. A dielectric constant of 1 was used for the electrostatic interactions, which were calculated by using the particle mesh Ewald method (18, 25). The grid in the x, y, and z directions used for the particle mesh Ewald method was set at 96, 80, and 108 points, respectively. The van der Waals interactions were described by using a Lennard–Jones function multiplied by a cubic spline switching function starting at 8 Å and stopping at 12 Å. The cut off radius for including atoms in the nearest-neighbor list was 13.5 Å. All 1–2 and 1–3 interactions were excluded, and 1–4 interactions were scaled by multiplication with a predefined factor. The bonded interactions were calculated every time step, the nonbonded interactions were calculated every other time step, and the electrostatic interactions were calculated every fourth time step. The nearest-neighbor list was updated every 20 time steps. Every 10 ps a snapshot was written to the trajectory file for subsequent analysis.

The hardware configuration used for these simulations was a Linux-based Beowulf cluster running on RedHat Linux 7.3 at either the Materials Process and Simulation Center at the California Institute of Technology or the Department of Biomedical Engineering at the Technische Universiteit Eindhoven. Each central processing unit in either of the two clusters was an Intel P4 2.2-GHz processor with 1 GB of memory. For each case (consisting of minimization and dynamics), a total of ≈5,800 processor hours was needed.

We thank Drs. Deepshikha Datta, Yashar Kalani, Spencer Hall, and Valeria Molinero for useful input and discussions and Dr. Koen Pieterse for some of the artwork. P.S. is the recipient of a Fulbright Scholarship supported by The Netherland–America Foundation and the Institute of International Education for research performed at the California Institute of Technology.

1. Giroux, M. & Ferrieres, J. (2003) *J. Asthma* **40,** 41–48.
2. Kobilka, B. (1992) *Annu. Rev. Neurosci.* **15,** 87–114.
3. Vaidehi, N., Floriano, W. B., Trabanino, R., Hall, S. E., Freddolino, P., Choi, E. J., Zamanakos, G. & Goddard, W. A., III (2002) *Proc. Natl. Acad. Sci. USA* **99,** 12622–12627.
4. Trabanino, R. J., Hall, S. E., Vaidehi, N., Floriano, W. B., Kam, V. W. T. & Goddard, W. A., III (2004) *Biophys. J.* **86,** 1904–1921.
5. Floriano, W. B., Vaidehi, N., Goddard, W. A., III, Singer, M. S. & Shepherd, G. M. (2000) *Proc. Natl. Acad. Sci. USA* **97,** 10712–10716.
6. Kalani, M. Y. S., Vaidehi, N., Freddolino, P. L., Hall, S. E., Trabanino, R. J., Floriano, W. B., Kam, V. W. T., Kalani, M. A. & Goddard, W. A., III (2004) *Proc. Natl. Acad. Sci. USA* **101,** 3815–3820.
7. Freddolino, P. L., Kalani, M. Y. S., Vaidehi, N., Floriano, W. B., Hall, S. E., Trabanino, R. J., Kam, V. W. T. & Goddard, W. A., III (2004) *Proc. Natl. Acad. Sci. USA* **101,** 2736–2741.
8. Hall, S. E., Floriano, W. B., Vaidehi, N. & Goddard, W. A., III (2004) *Chem. Senses* **29,** 595–616.
9. Hummel, P., Vaidehi, N., Floriano, W. B., Hall, S. E. & Goddard, W. A., III (2005) *Protein Sci.* **14,** 703–710.
10. Kobilka, B. (2004) *Mol. Pharmacol.* **65,** 1060–1062.
11. Devanathan, S., Yao, Z., Salamon, Z., Kobilka, B. & Tollin, G. (2004) *Biochemistry* **43,** 3280–3288.
12. Swaminath, G., Xiang, Y., Lee, T. W., Steenhuis, J., Parnot, C. & Kobilka, B. K. (2004) *J. Biol. Chem.* **279,** 686–691.
13. Kobilka, B. K. (2002) *J. Peptide Res.* **60,** 317–321.
14. Liapakis, G., Chan, W. C., Papadokostaki, M. & Javitch, J. A. (2004) *Mol. Pharmacol.* **65,** 1181–1190.
15. Humphrey, W., Dalke, A. & Schulten, K. (1996) *J. Mol. Graphics* **14,** 33–38.
16. Patel, A. B., Crocker, E., Reeves, P. J., Getmanova, E. V., Eilers, M., Khorana, H. G. & Smith, S. O. (2005) *J. Mol. Biol.* **347,** 803–812.
17. Yamano, Y., Kamon, R., Yoshimizu, T., Toda, Y., Oshida, Y., Chaki, S., Yoshioka, M. & Morishima, I. (2004) *Biosci. Biotechnol. Biochem.* **68,** 1369–1371.
18. Brooks, B. R., Bruccoleri, R. E., Olafson, B. D., States, D. J., Swaminathan, S, & Karplus, M. (1983) *J. Comp. Chem.* **4,** 187–217.
19. MacKerell, A. D., Jr., Bashford, D., Bellott, M., Dunbrack, R. L., Jr., Evanseck, J. D., Field, M. J., Fischer, S., Gao, J., Guo, H., *et al.* (1998) *J. Phys. Chem. B* **102,** 3586–3616.
20. Feller, S. E. & MacKerell, A. D., Jr. (2000) *J. Phys. Chem. B* **104,** 7510–7515.
21. Mayo, S. L., Olafson, B. D. & Goddard, W. A., III (1990) *J. Phys. Chem.* **94,** 8897–8909.
22. Gasteiger, J. & Marsili, M. (1980) *Tetrahedron* **36,** 3219–3228.
23. Nelson, M., Humphrey, W., Gursoy, A., Dalke, A., Kale, L., Skeel, R. D. & Schulten, K. (1996) *Int. J. Supercomput. Appl. High Perform. Comput.* **10,** 251–268.
24. Kale, L., Skeel, R., Bhandarkar, M., Brunner, R., Gursoy, A., Krawetz, N., Phillips, J., Shinozaki, A., Varadarajan, K. & Schulten, K. (1999) *J. Comp. Phys.* **151,** 283–312.
25. Bhandarkar, M., Brunner, R., Chipot, C., Dalke, A., Dixit, S., Grayson, P., Gullingsrud, J., Gursoy, A., Hardy, D., Humphrey, W., *et al.* (2003) NAMD *User's Guide* (Theoretical Biophysics Group, University of Illinois at Urbana–Champaign and Beckman Institute, Urbana), Version 2.5.